ACS APPLIED ENERGY MATERIALS

www.acsaem.org Article

Manipulation of PEDOT:PSS with Polar and Nonpolar Solvent Post-treatment for Efficient Inverted Perovskite Solar Cells

Zhiyin Niu, Erjin Zheng, Hao Dong, Gabriella A. Tosado, and Qiuming Yu*

Cite This: *ACS Appl. Energy Mater.* 2020, 3, 9656−9666 Read Online

ACCESS | Metrics & More | Article Recommendations | Supporting Information

ABSTRACT: Poly(3,4-ethylenedioxythiophene):poly(styrene sulfonate) (PEDOT:PSS) has been widely used as a hole-conducting polymer in many optoelectronic devices including perovskite solar cells. However, its electrical and surface properties are not well controlled during the conventional ambient annealing. Herein, we apply the solvent post-treatments, including toluene vapor annealing and ethylene glycol (EG) washing, to modify not only the electrical conductivity and work function but also, importantly, the surface composition and morphology of PEDOT:PSS thin films. We show that annealing PEDOT:PSS films in a nonpolar toluene vapor environment results in a slightly enhanced electrical conductivity and increased work function while maintaining the surface composition and morphology. The $CH_3NH_3PbI_3$ perovskite solar cells using the toluene vapor-annealed PEDOT:PSS hole transporting layers (HTLs) yield a 31.8% increase in power conversion efficiency (PCE) from the control devices with the ambient condition-annealed PEDOT:PSS HTLs. All photovoltaic parameters are increased because of reduced trap states at the perovskite/HTL interface, as well as efficient and balanced charge generation, transport, and extraction rates. In contrast, washing PEDOT:PSS films with the polar EG solvent removes the PSS on the surface, increases the surface roughness, and dramatically increases the electrical conductivity by 5 orders of magnitude but slightly decreases the work function. Consequently, the $CH_3NH_3PbI_3$ perovskite solar cells with EG-washed PEDOT:PSS HTLs result in a 28.6% decrease in PCE from the control devices because of the increased trap states at the perovskite/HTL interface, which leads to an inefficient hole extraction. The charge accumulation at the perovskite/HTL interface also reflects in a serious hysteresis of *J*−*V* curves in the reversed bias region. This work highlights the importance of controlling both electronic and surface properties of PEDOT:PSS HTLs for the improvement of perovskite solar cell performance.

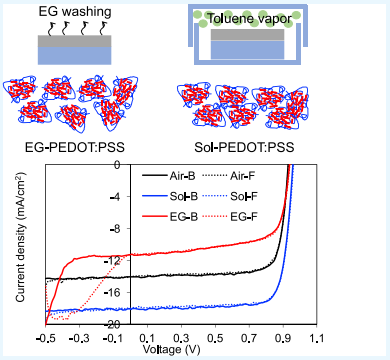

KEYWORDS: *solvent annealing, hole transport material, perovskite, solar cell, PEDOT:PSS*

INTRODUCTION

Hybrid perovskite solar cells show great potentials as a renewable energy source because of the exceptional optoelectronic properties of perovskites including strong light absorption,[1] high charge carrier mobility and lifetimes,[2,3] long ambipolar carrier diffusion lengths,[4,5] and the low-cost, large area solution processability. Power conversion efficiency (PCE) of perovskite solar cells has been dramatically improved to over 20%[6] from 3.8%[7] since 2009. Perovskite solar cells with an inverted p−i−n architecture have a perovskite photoactive layer (i) sandwiched between a hole transport layer (HTL, p) and an electron transport layer (ETL, n) with the HTL built on top of the transparent anode. The capability of solution processing of each layer at moderate temperatures makes the inverted structured perovskite solar cells more attractive for commercialization.[8,9]

Poly(3,4-ethylenedioxythiophene):poly(styrene sulfonate) (PEDOT:PSS) has been widely used as a hole conducting polymer in many optoelectronic devices, such as light-emitting diodes (LEDs),[10] photodetectors,[11,12] and solar cells.[8,9] Spin-cast PEDOT:PSS films are known to have core−shell domains.[13,14] The core is a composite of hole-conducting, short-oxidized PEDOT chains (typically 5−10 repeat units)[10] doped by polyelectrolyte PSS counter ions, and the shell is formed by excess, nonconductive PSS with a thickness of around 3−4 nm.[15,16] Therefore, the electrical conductivity and work function of a PEDOT:PSS film, which are critical to perovskite solar cell performance, strongly depend on the microstructures and morphologies of PEDOT:PSS domains in the film. The weight ratio of PSS and PEDOT is also a critical factor as it directly affects the electrical conductivity and work function of PEDOT:PSS films. The highly conducting grade PEDOT:PSS (*CLEVIOS* PH 1000) with a 2.5:1 PSS to PEDOT weight ratio has an electrical conductivity in the order of 10^{-1} S/cm but relatively large energy mismatches with most

Received: May 22, 2020
Accepted: September 18, 2020
Published: September 18, 2020

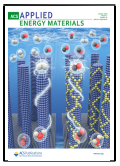

https://dx.doi.org/10.1021/acsaem.0c01194
ACS Appl. Energy Mater. 2020, 3, 9656−9666

photoactive materials.[17] Various processing methods have been developed to either modify the microstructures or reduce the PSS amount to further enhance the electrical conductivity of PH1000 PEDOT:PSS by 2−4 orders of magnitude for a variety of applications of conducting polymers, including the replacement of transparent conductive oxides as electrodes for flexible solar cells.[18−23] PH1000 PEDOT:PSS has also been used as HTLs. Adding poly-(ethylene glycol) (PEG), ethylene glycol (EG), or dimethyl sulfoxide (DMSO) into PH1000 PEDOT:PSS emulsions or ultrasonication-treating PH1000 PEDOT:PSS emulsions facilitates the rearrangement of PSS in the spin-cast PEDOT:PSS films, which varies the electrical conductivity, resulting in the improved performance of the perovskite, polymer, and planar silicon solar cells.[24−26]

The commercial PEDOT:PSS (*CLEVIOS* P VP AI 4083) with a 6:1 PSS to PEDOT weight ratio has a suitable work function as an HTL for most polymer and perovskite solar cells, but its strong acidity and low electrical conductivity due to the increased PSS content have direct impacts on device performance and stability. Various methods have been explored to neutralize acidity, modify PEDOT and PSS domain structures, or reduce the PSS amount. Adding bases to AI 4083 PEDOT:PSS not only neutralizes its acidity but also modifies its optical and electronic properties. It was found that strong base like NaOH dedoped the PEDOT:PSS and decreased the work function because of the change in relative stability of oxidized thiophene units induced by the replacement of PSS-H with PSS-Na, which adversely affects hole injection in polymer LEDs.[10] Using an organic mild base, imidazole, to increase the pH from 2.2 to 9, the basic PEDOT:PSS maintained 90% of its original electrical conductivity while increasing the work function to −5.3 eV, closer to the valence band maximum (−5.43 eV) of the $CH_3NH_3PbI_3$ perovskite. The basic PEDOT:PSS HTL resulted in a marked increase in PCE of the inverted $CH_3NH_3PbI_3$ perovskite solar cell from 12.7 to 15.7% because of a significantly enlarged open-circuit voltage (V_{OC}) from 0.88 to 1.06 V.[27] Organic solvents have been explored to add into AI 4083 PEDOT:PSS emulsions and deployed the modified PEDOT:PSS as an HTL in organic and perovskite solar cells.[28,29] The cosolvent of polar methanol and nonpolar 1,2-dichlorobenzene (DCB) was shown to significantly increase the PEDOT:PSS electrical conductivity by 3 orders of magnitude to ∼10 S/cm because of the morphology changes induced by the preferential solvation of hydrophobic PEDOT and hydrophilic PSS with the two components of the cosolvent. The greatly enhanced electrical conductivity slightly improved the short-circuit current density (J_{SC}) while no improvements in the V_{OC} and fill factor (FF), resulting in a limited increase in PCE from 3.98 to 4.31% of the organic solar cells.[29] A single polar DMSO solvent was added in AI 4083 PEDOT:PSS emulsions, and the modified PEDOT:PSS was used as an HTL in the $CH_3NH_3PbI_3$ perovskite solar cells.[28] An apparent increase in PCE from 12.2 to 16.7% was achieved with the DMSO-treated PEDOT:PSS HTL compared to the pristine PEDOT:PSS, which is mainly because of the increase in J_{SC} while no changes in V_{OC} and FF. Despite a minor electrical conductivity increase and even a slight drop in work function to −4.9 eV, the enhanced J_{SC} was attributed to the two positive impacts of the DMSO-treated PEDOT:PSS: the efficient pathway of hole extraction and transport and the modulation of the $CH_3NH_3PbI_3$ crystal growth with improved morphology and crystallinity.

Instead of adding solvents or chemicals into PEDOT:PSS emulsions, various methods have also been developed to treat PEDOT:PSS films during or post annealing. Spin-coating sodium citrate solution on the preannealed PEDOT:PSS partially removed PSS from the surface, resulting in the increased J_{SC} and V_{OC} of $CH_3NH_3PbI_3$ perovskite solar cells.[30] The sodium citrate-treated PEDOT:PSS HTLs promoted the growth of large perovskite crystalline grains and enhanced charge collection. $CH_3NH_3PbI_3$ perovskite solar cells with the PEDOT:PSS HTLs, treated with propionic acid (PA) and blowing nitrogen gas during annealing, exhibited an increased V_{OC} from 0.842 to 0.877 V because of the reduced charge carrier recombination at the PA-treated PEDOT:PSS/perovskite interface.[31] Polar organic solvents, such as DMSO, dimethylformamide (DMF), g-butyrolactone (GBL), or their cosolvents, are commonly used in preparing perovskite precursor solutions. The effect of PEDOT:PSS films treated with these solvents was investigated, and no significant impact was observed on the device performance.[32−34] However, the perovskite precursor methylammonium iodide (MAI) in DMF or DMSO was found to play a critical role in removing PSS from the PEDOT:PSS surface, which increased the surface roughness and electrical conductivity from 10^{-3} to 10^{1} S cm^{-1} but lowered the device performance.[32] Stronger polar solvents, such as water, ethanol, or their mixtures, were spin-coated on the preannealed PEDOT:PSS films.[34,35] PSS was partially removed from the surface and the electrical conductivity was increased, but inferior device performance was shown. Spin-coating PSSNa on the treated PEDOT:PSS films restored the PSS content on the surfaces and the device performance was recovered, indicating the importance of having PSS on PEDOT:PSS surfaces. However, recent studies showed that significantly reducing PSS on PEDOT:PSS surfaces improved the device performance. Deploying PEDOT:PSS HTLs, treated by sequentially dipping the PEDOT:PSS films in EG and methanol, in the $CH_3NH_3PbI_3$ perovskite solar cells not only enhanced all photovoltaic parameters but also improved device stability.[36] Dipping the PEDOT:PSS films in EG helps in forming hydrogen bonds between EG and PSS and makes PEDOT conformation change from coil-like to linear. The subsequent dipping in methanol removes PSS and EG from the surfaces, resulting in PEDOT-rich films, which benefits the charge transport and device stability. Recent studies even showed that drop-casting ultrapure water on the preannealed PEDOT:PSS film yielded a monolayer of PEDOT:PSS on an indium tin oxide (ITO)/glass substrate with PSS attached to ITO via In−O−S chemical bonds and PEDOT on the surface.[37] All photovoltaic parameters were increased, and a PCE of 18.0% was achieved in comparison to 13.4% for the device with a control PEDOT:PSS HTL made by conventional annealing. Apparently, apart from electrical conductivity and work function, surface properties of PEDOT:PSS films could have a remarkable impact on perovskite solar cell performance, and further investigations are highly desired.

In this work, we apply the solvent post-treatments, including the nonpolar toluene vapor annealing and polar EG washing, to modify not only the electrical conductivity and work function but also, importantly, the surface composition and morphology of AI 4083 PEDOT:PSS thin films. We show that annealing PEDOT:PSS films in a nonpolar toluene vapor environment allows a slow rearrangement of PEDOT and PSS domains, resulting in a slightly enhanced electrical conductivity and increased work function, while maintaining the surface

https://dx.doi.org/10.1021/acsaem.0c01194
ACS Appl. Energy Mater. 2020, 3, 9656−9666

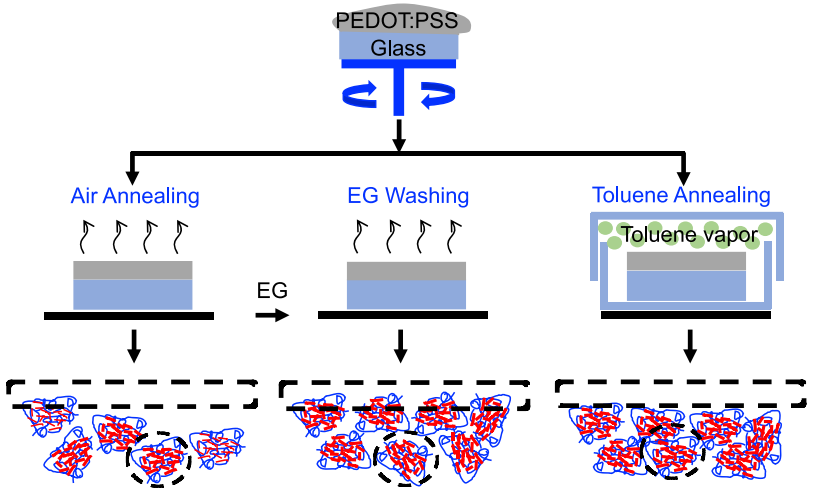

Figure 1. Schematics of post-treatment processes and the resulting conformations of PEDOT:PSS thin films. The long blue and short red curves stand for PSS and PEDOT chains, respectively, which are the hole-conducting cores. The light blue background represents nonconductive shells formed by excess PSS. The dashed black boxes indicate the microstructure and morphology near the surface.

composition and morphology. As a result, the $CH_3NH_3PbI_3$ perovskite solar cells using the toluene vapor-annealed PEDOT:PSS HTLs yield a 31.8% increase in PCE from the control devices with the ambient condition-annealed PEDOT:PSS HTLs. All photovoltaic parameters are increased because of reduced trap states at the perovskite/HTL interface, as well as efficient and balanced charge generation, transport, and extraction rates. In contrast, washing preannealed PEDOT:PSS films with the polar EG solvent removes PSS on the surface, increases the surface roughness, and dramatically increases the electrical conductivity by 5 orders of magnitude but slightly decreases the work function. Consequently, the $CH_3NH_3PbI_3$ perovskite solar cells using the EG-washed PEDOT:PSS HTL result in a 28.6% decrease in PCE from the control devices. The decreases in J_{SC} and FF are attributed to the increased trap states at the perovskite/HTL interface, which leads to an inefficient hole extraction. The charge accumulation at the perovskite/HTL interface also reflects in a serious hysteresis of $J-V$ curves in the reversed bias region. This work highlights the importance of controlling both electronic and surface properties of PEDOT:PSS HTLs for the improvement of perovskite solar cell performance.

RESULTS AND DISCUSSIONS

Solvent Post-treatment of PEDOT:PSS Thin Films. The spin-casted PEDOT:PSS thin films are typically annealed under the ambient condition at >120 °C for a certain length of time. As illustrated in Figure 1, we prepared the control PEDOT:PSS thin films by annealing in air at 120 °C for 25 min. The solvent post-treated PEDOT:PSS films were prepared by annealing in toluene vapor at 120 °C for 25 min or spin-casting EG on preannealed PEDOT:PSS films followed by annealing in air at 120 °C for another 10 min, which is referred to EG washing PEDOT:PSS. We attempt to manipulate the nonequilibrium process during annealing using solvents that have different hydrophobicities. When deposited from aqueous dispersion, instead of reaching an equilibrium state in the solid film, PEDOT:PSS polymer domains are "frozen" in nonequilibrium states.[38−40] Annealing in air with the temperature higher than the boiling point of water evaporates water molecules from the PEDOT:PSS film, forming a core−shell structure with excess PSS on the surface because of the hydrophilic nature of the ambient condition. Washing the preannealed PEDOT:PSS film with EG removes the excess surface PSS because of the hydrophilic property of EG with a dielectric constant of 37. EG molecules are left behind in the PEDOT:PSS film after washing. Because the boiling point of EG is 197 °C, almost double the boiling point of water, the hydrophilic EG molecules stay in the film even longer than water molecules during the second annealing process, causing the segregation of PSS and PEDOT domains.[19,26,41] Toluene, as a nonpolar solvent, has a low dielectric constant of 2.38 and a boiling point of 111 °C. Annealing at 120 °C with toluene vapor allows hydrophobic toluene molecules interact with hydrophobic PEDOT, inducing the rearrangement of PEDOT and PSS microstructures, especially close to the surface.

To investigate the influence of solvent post-treatments on surface properties of PEDOT:PSS films, we conducted the water contact angle measurements and acquired the AFM images (Figure 2). The significant difference in hydrophobicity between PEDOT and PSS makes the measurement of the water contact angle on a PEDOT:PSS surface a quick method to detect the changes in the relative amount of PEDOT and PSS on the surface. A small water contact angle of 7.7° of the air-annealed surface indicates that the surface is mainly

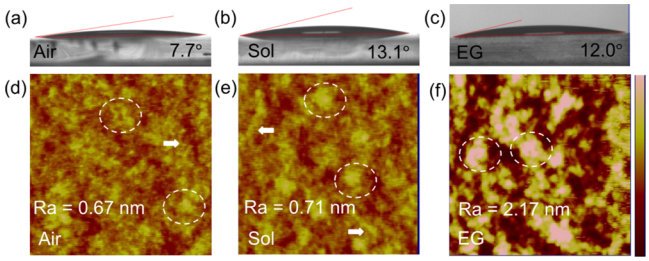

Figure 2. Contact angle of water on PEDOT:PSS films prepared with (a) air annealing, (b) toluene vapor annealing, and (c) EG washing, along with their topographic AFM images displayed in (d−f), respectively. The circles and arrows in (d−f) mark the PEDOT clusters and chainlike nanostructures, respectively. AFM image size is 1 μm × 1 μm, and the Z scale is 10 nm.

https://dx.doi.org/10.1021/acsaem.0c01194
ACS Appl. Energy Mater. 2020, 3, 9656−9666

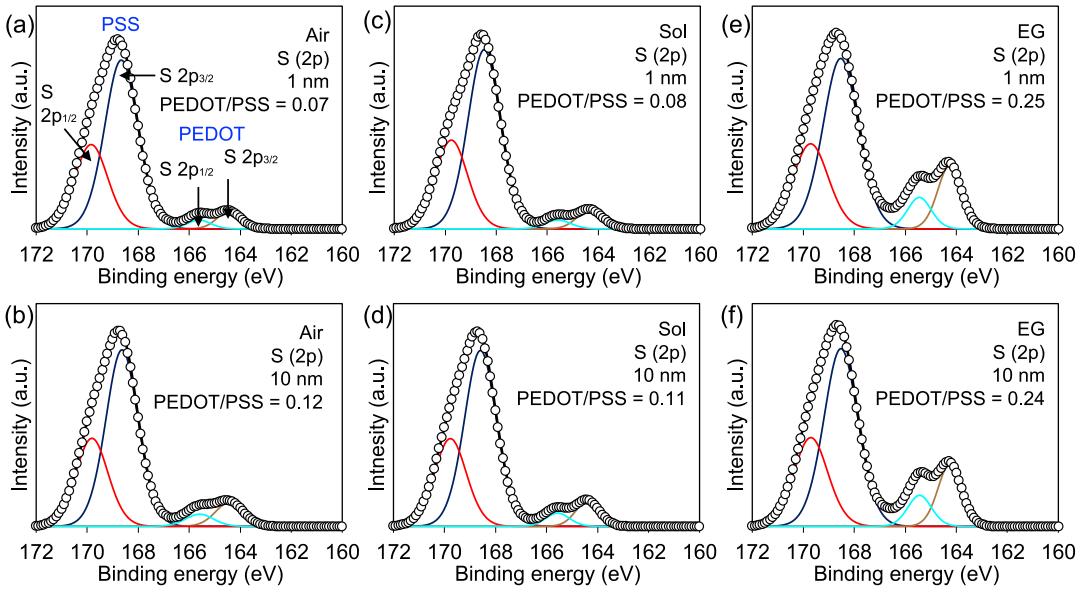

Figure 3. XPS spectra of S 2p of PEDOT:PSS thin films prepared with air annealing, toluene vapor annealing, and EG washing. The electron takeoff angle is 70° for the spectra shown in (a, c, and e) and 0° in (b, d, and f), corresponding to the electron escape depth of 1 and 10 nm, respectively.

occupied by the hydrophilic PSS (Figure 2a). The water contact angle increases to 13.1 and 12.0° after toluene vapor annealing and EG washing (Figure 2b,c), suggesting that more hydrophobic PEDOT chains segregate to the surfaces but the surfaces are still dominated by the hydrophilic PSS. The increase in water contact angle was observed on the PEDOT:PSS surfaces in which PSS was partially removed.[36,37]

The AFM images show that both air-annealed and toluene vapor-annealed PEDOT:PSS films are highly smooth with the surface roughness less than 1 nm (Figure 2d,e). The toluene vapor-annealed PEDOT:PSS surface is slightly rougher and has more agglomeration of oblate ellipsoidal-shaped PEDOT nanocrystals,[26] marked in dashed circles. Chainlike nanostructures, marked in arrows, remain clear after toluene vapor annealing but become obscured after EG washing. EG washing produces a rough surface and closely packed PEDOT nanocrystals with enlarged size (Figure 2f), which is ascribed to the removal of PSS from PEDOT:PSS surfaces.[23,30,32−34]

To quantitatively characterize the surface chemical composition of PEDOT:PSS films prepared with different methods, we performed the XPS studies and changed the electron takeoff angle from the normal 0 to 70°, corresponding to the electron escape depth of 10 and 1 nm, respectively. The typical S 2p spectra of PEDOT:PSS with and without solvent post-treatment are shown in Figure 3a−f. The spectra show two S 2p bands, each corresponding to a doublet of S $2p_{3/2}$ and S $2p_{1/2}$ components with 1.2 eV spin−orbit splitting and a 2:1 intensity ratio. The sulfur signal for PSS appears at higher binding energy (168−169 eV) because of the three electronegative oxygen attachments in the sulfonate moiety withdrawing the electron density of the sulfur atom. The S 2p doublet at 164−165 eV comes from the sulfur atom of the PEDOT.[22,38] The ratio of the S $2p_{3/2}$ peak area for PEDOT and PSS is used to estimate the relative composition of PEDOT and PSS on the surface, and the value is displayed in each corresponding figure. The lowest PEDOT/PSS ratio of 0.07 is found for the top 1 nm of the air-annealed PEDOT:PSS surface (Figure 3a), and the ratio is increased to 0.12 when the electron escape depth is increased to 10 nm (Figure 3b), indicating that PSS is predominantly the top surface of air-annealed PEDOT:PSS and the PEDOT content increases in the underneath surface. These PEDOT/PSS ratios are in a good agreement with the literature values of 0.09−0.20 for air-annealed PEDOT:PSS.[30,34−36] The similar PEDOT/PSS ratios at 1 and 10 nm probe depths of toluene vapor-annealed PEDOT:PSS (Figure 3c,d) suggest that the surface chemical composition remains almost the same and the surface is still dominated by PSS, even though toluene molecules induce the rearrangement of PEDOT and PSS domains shown by AFM and contact angle measurements. EG washing dramatically increases the PEDOT/PSS ratio to 0.25 in the top 1 nm surface, and this ratio remains the same in the top 10 nm surface (Figure 3e,f), indicating that EG molecules effectively remove PSS from the surface and create a relatively uniform chemical composition in the top 10 nm surface. The PEDOT to PSS ratios were reported to be 0.30, 0.25, and 0.24 for the PEDOT:PSS films treated with DMF, DMSO, and EG washing, respectively,[34] which are consistent with our results. Both XPS and AFM results indicate that PSS shells are partially removed by EG washing.

The change in the surface composition is further confirmed by C 1s spectra, shown in Figure S1. The peak fitting of core-level C 1s is shown in Figure S1a−f for the air-annealed, toluene vapor-annealed, and EG-washed PEDOT:PSS films with normal and high electron takeoff angles, respectively. The spectra for all samples displayed three components with binding energies at 285.0, 286.5, and 287.8 eV, corresponding to C−H/C−C, C−O, and C−S of PEDOT:PSS, respectively.[42] In comparison to the C 1s spectra of the air-annealed PEDOT:PSS film, the film treated with toluene vapor annealing shows insignificant changes, while the EG-washed film develops an obvious difference in the C 1s spectra, where the high-binding energy side of the main peak, representing the C−S and C−O, exhibits a consistent enlargement in intensity in both top 1 and 10 nm surfaces. This is indicative that the outermost surface of the PEDOT:PSS film becomes rich in

https://dx.doi.org/10.1021/acsaem.0c01194
ACS Appl. Energy Mater. 2020, 3, 9656−9666

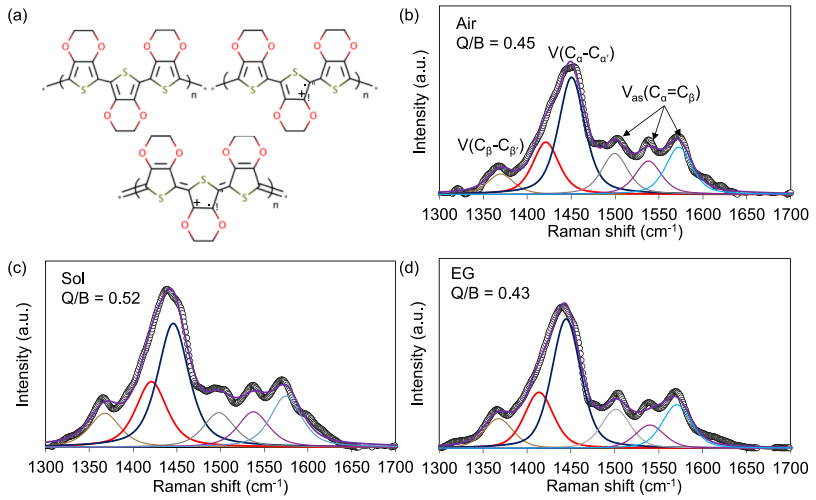

Figure 4. (a) PEDOT with different doping levels and structures. Top two: neutral and oxidized PEDOT with a benzoid structure; bottom: oxidized PEDOT with a quinoid structure. (b–d) Raman spectra of PEDOT:PSS thin films prepared with air annealing, toluene vapor annealing, and EG washing, respectively.

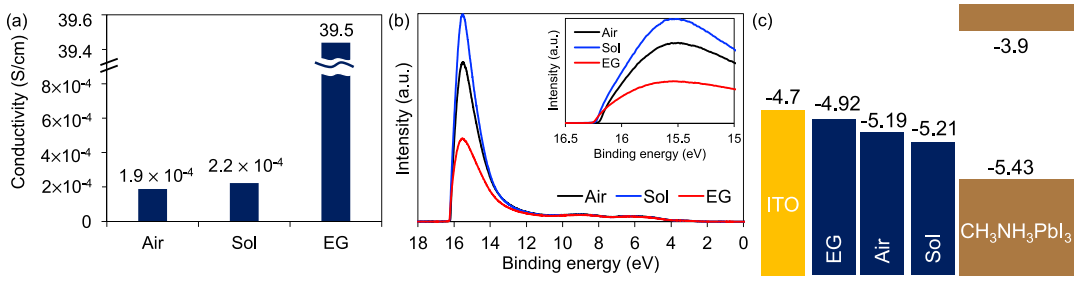

Figure 5. (a) Electrical conductivity and (b) UPS spectra of PEDOT:PSS films prepared by air annealing, toluene vapor annealing, and EG washing. The inset in (b) shows the corresponding secondary electron cutoff. (c) Energy diagram showing the work function of ITO and PEDOT:PSS thin films and the valence band maximum and conduction band minimum of $CH_3NH_3PbI_3$. All the energy levels are in a unit of eV.

carbonyl carbon after EG washing, which suggests that there are more PEDOT grains on the top surface of the EG-washed film.

Although the XPS analysis provides the surface chemical composition, UV–vis absorption spectroscopy could show the change in the entire films. The UV–vis absorption spectrum of the EG-washed PEDOT:PSS film shows a dramatic intensity decrease of the peak at ~230 nm originated from the aromatic rings of PSS (Figure S2). The decrease in the PSS absorption peak was also observed for the PEODT:PSS films treated with polar solvents.[32,35−37] The PSS absorption peak of the toluene vapor-annealed PEDOT:PSS film also decreases slightly, which is consistent with the XPS results.

It is known that the PEDOT chain has a benzoid structure in its reduced state and both quinoid and benzoid structures in its oxidized state (Figure 4a). To further study the chemical state and structure of PEDOT in the PEDOT:PSS films treated with different solvent post-treatments, we acquired the Raman spectra of PEDOT:PSS films and deconvoluted the spectra between 1300 and 1700 cm^{-1} (Figure 4b–d). The peaks at 1361, 1440, 1504, and 1570 cm^{-1} are assigned to the $C_\beta = C_{\beta'}$ vibration, $C_\alpha = C_\beta$ symmetric stretching vibration, and $C_\alpha = C_\beta$ asymmetric stretching vibrations, respectively.[43−45] The inconspicuous peak centered at 1534 cm^{-1} arises from the splitting of the asymmetric vibrations and only presents if the PEDOT is highly oxidized.[46] The 1440 cm^{-1} peak can be deconvoluted into two separated bands, centered at 1414 and 1445 cm^{-1}, because of the $C_\alpha = C_\beta$ symmetrical stretching in quinoid and benzoid structures, respectively. We calculated the quinoid to benzoid ratio (Q/B) from these peak areas. The Q/B ratio of the toluene vapor-annealed PEDOT:PSS is 0.52, higher than the values of 0.45 and 0.43 of the air-annealed and EG-washed films, respectively. The increase in Q/B ratio indicates that toluene vapor annealing helps with the change in PEDOT chains from a more coil-like benzoid structure to a more linear or extended quinoid structure, allowing closely packing PEDOT chains, which facilitates hole transport.[36] The expansion of PEDOT chains is believed to cause the size increase in PEDOT nanocrystals observed in the AFM images.[26] In contrast, EG washing simply removes excess PSS but has no impact on the PEDOT structure. This is because EG only has a very short time to interact with PSS during spin casting. Adding EG into PEDOT:PSS emulsions or dipping PEDOT:PSS films into the EG solvent allows a much longer time for EG molecules to interact with PSS, which facilitates the formation of hydrogen bonds between EG and PSS and induces the conformation change in PEDOT.[36,37]

Figure 5a shows the electrical conductivity of air-annealed, toluene vapor-annealed, and EG-washed PEDOT:PSS films. The electrical conductivity of the toluene vapor-annealed PEDOT:PSS film increases slightly to 2.2×10^{-4} from 1.9×10^{-4} S/cm of the air-annealed film, while about 5 orders of magnitude increase is shown by the EG-washed film. The work function of three PEDOT:PSS films was obtained from the UPS study (Figure 5b and Table S1). The work function of the air-annealed PEDOT:PSS film is −5.19 eV, similar to ~−5.2

https://dx.doi.org/10.1021/acsaem.0c01194
ACS Appl. Energy Mater. 2020, 3, 9656−9666

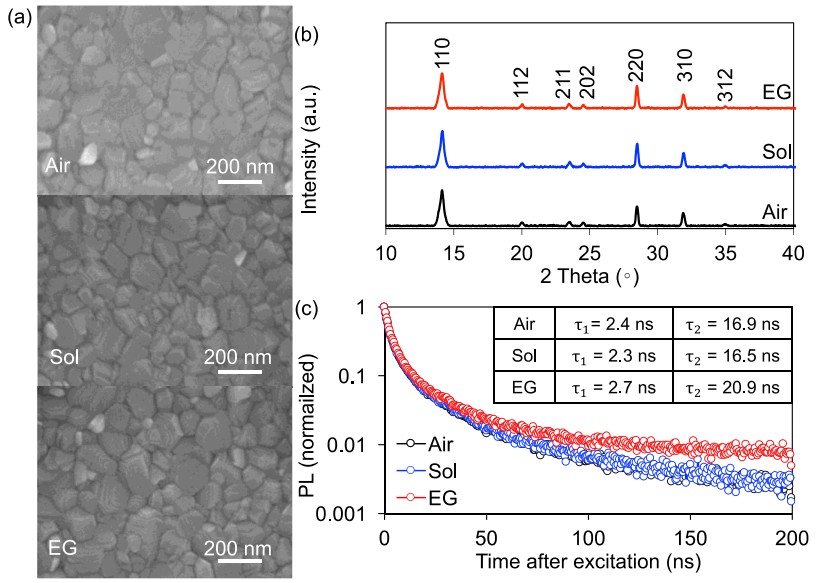

Figure 6. (a) Top-view SEM images, (b) XRD patterns, and (c) TRPL lifetime of $CH_3NH_3PbI_3$ films fabricated atop PEDOT:PSS thin films prepared with air annealing, toluene vapor annealing, and EG washing. The corresponding TRPL lifetimes are displayed in (c).

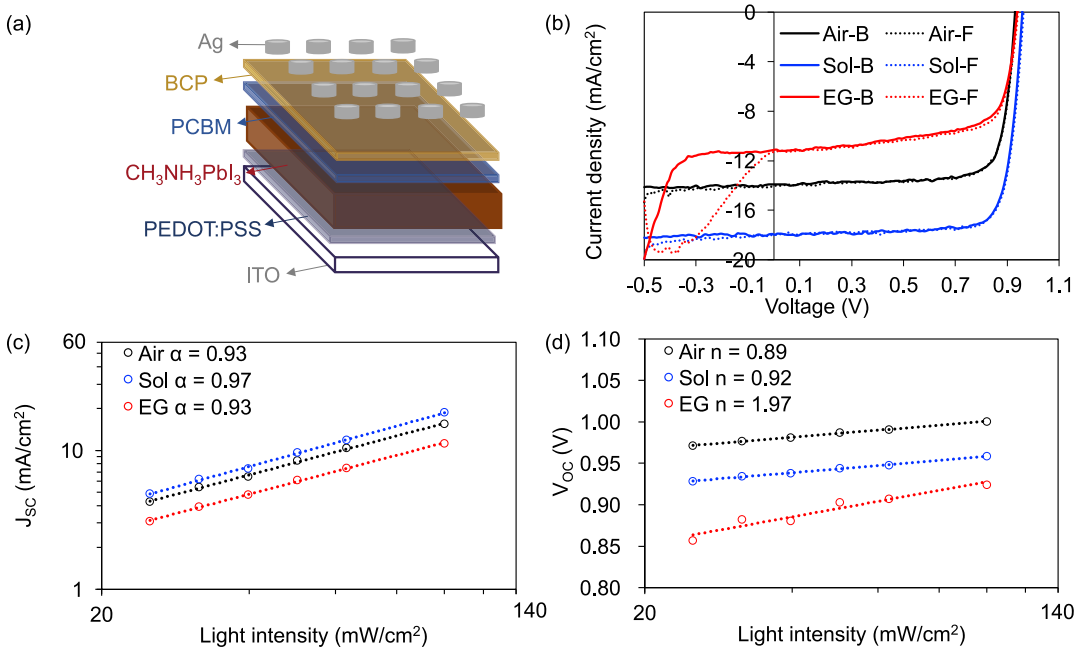

Figure 7. (a) Illustration of an inverted device structure with a $CH_3NH_3PbI_3$ active layer. (b) $J-V$ characteristics, (c) J_{SC} as a function of light intensity in a double logarithmic scale, and (d) V_{OC} as a function of light intensity in a semilogarithmic scale for $CH_3NH_3PbI_3$ solar cells with the PEDOT:PSS HTLs prepared with air annealing, toluene vapor annealing, and EG washing. Forward $J-V$ scan is from −0.5 to 1.5 V with a scan rate of 0.01 V/s.

eV reported in the literature.[11,12,27] Toluene annealing increases the work function to −5.21 eV, which is closer to the valence band maximum (VBM) −5.43 eV of $CH_3NH_3PbI_3$. In contrast, EG washing decreases the work function to −4.92 eV, resulting in a larger energy mismatch between PEDOT:PSS and the VBM of $CH_3NH_3PbI_3$. We used the four-point probe method to measure electrical conductivity. Therefore, the electrical conductivity is very sensitive to the PSS content in the top surface region. Partial removal of PSS with polar solvents results in a dramatic increase in electrical conductivity, while a slight reduction in the work function of PEDOT:PSS.[23,32]

$CH_3NH_3PbI_3$ Perovskite Films on Air-Annealed and Solvent Post-treated PEDOT:PSS Thin Films. We used the one-step solution process with antisolvent wash to fabricate the $CH_3NH_3PbI_3$ perovskite thin films on the PEDOT:PSS films prepared in three methods. SEM images show almost identical surface morphology and grain size for all perovskite films (Figures 6a and S3), which is consistent with the previous results.[30,33] The thin films are composed of grains with stacked body-centered tetragonal lattice layers with sharply faceted rhombo-hexagonal dodecahedra. XRD patterns, in Figure 6b, show the peaks at 14.2, 23.6, 28.3, and 31.7°, corresponding to the (110), (211), (220), and (310) crystal planes of the

https://dx.doi.org/10.1021/acsaem.0c01194
ACS Appl. Energy Mater. 2020, 3, 9656−9666

Table 1. Photovoltaic Parameters of $CH_3NH_3PbI_3$ Solar Cells With PEDOT:PSS HTLs Prepared With Air Annealing, Toluene Vapor Annealing, and EG Washing[a]

PEDOT:PSS	V_{OC} (V)	J_{SC} (mA/cm^2)	FF	PCE (%)	R_S (Ω cm^2)	R_{sh} (Ω cm^2)
air	0.94 ± 0.02 (0.93)	13.03 ± 1.00 (14.00)	0.79 ± 0.02 (0.80)	9.72 ± 0.80 (10.35)	10.92	626.40
sol	0.97 ± 0.02 (0.96)	16.64 ± 1.90 (17.81)	0.76 ± 0.04 (0.80)	12.27 ± 1.37 (13.64)	11.42	1139.16
EG	0.94 ± 0.02 (0.94)	11.20 ± 0.10 (11.27)	0.62 ± 0.08 (0.70)	6.46 ± 0.38 (7.39)	4.83	128.95

[a]The photovoltaic parameters of the best performance devices are in parenthesis. The series resistance R_S and shunt resistance R_{sh} are calculated from the best performance devices.

tetragonal ($I4/mcm$) phase of the $CH_3NH_3PbI_3$ thin films.[31,47] There is no obvious difference in the intensity and full width at half-maximum (fwhm) of diffraction peaks, implying that the crystallinity is almost identical for the perovskite films fabricated on air-annealed, toluene vapor-annealed, and EG-washed PEDOT:PSS films. The UV−vis absorption spectra show that all three $CH_3NH_3PbI_3$ thin films have the same absorption edge around 780 nm (Figure S4). All these results show that the solvent post-treated PEDOT:PSS films have no obvious impacts on the morphology, crystallinity, and optical band gap of $CH_3NH_3PbI_3$ thin films fabricated atop of them.

To investigate the morphology and composition change of PEDOT:PSS thin films on charge extraction from the atop perovskite films, we characterized the charge carrier lifetime using time-resolved photoluminescence (TRPL). We compared the transient fluorescence decays from the PL peak at 760 nm for three $CH_3NH_3PbI_3$ films (Figure 6c). Biexponential fitting (eq 1) reveals both fast and slow dynamics, with the fast component lifetime (τ_1) values and the slow component lifetime (τ_2) values listed in the inset of Figure 6c.

$$I(t) = A_1 \exp\left(\frac{t}{\tau_1}\right) + A_2 \exp\left(\frac{t}{\tau_2}\right) \quad (1)$$

The fast decay component is closely related to nonradiative recombination by defects of surface traps near grain boundaries, and the slow decay component is related to radiative recombination from bulk perovskite.[48] Because the perovskite films are made on top of the PEDOT:PSS HTLs, their PL lifetimes are also related to the effectiveness of hole extraction by the underneath HTLs. Perovskite films made on top of the air-annealed and toluene vapor-annealed PEDOT:PSS HTLs exhibit similar fast and slow decay times, indicating similar hole extraction capabilities of both PEDOT:PSS HTLs, which is consistent with their similar surface morphology and composition. Both fast and slow decay times are the longest for the perovskite film made on the EG-washed PEDOT:PSS, indicating that photon-generated holes cannot be effectively extracted by this HTL. Even though a rough and increased PEDOT content surface, which is generated by EG washing, does not affect the morphology, crystallinity, and optical band gap of the $CH_3NH_3PbI_3$ perovskite film grown atop, it is inferior to hole extraction.

$CH_3NH_3PbI_3$ Perovskite Solar Cells with Air-Annealed and Solvent Post-treated PEDOT:PSS HTLs. We deployed the PEDOT:PSS prepared in three methods in the planar structured solar cells with the structure of glass/ITO/PEDOT:PSS/$CH_3NH_3PbI_3$/$PC_{60}BM$/BCP/Ag, as illustrated in Figure 7a. All three PEDOT:PSS films show close to a unity transmittance in the wavelength longer than 400 nm (Figure S5). Figure 7b shows the current density−voltage ($J-V$) characteristics of the best performance solar cells. The average and the best performance photovoltaic parameters are summarized in Table 1. The series resistance R_S and shunt resistance R_{sh} of the best performance devices were calculated with the equations in the Supporting Information, which are also summarized in Table 1. The best performance device with the toluene vapor-annealed PEDOT:PSS HTL achieves a J_{SC} of 17.81 mA cm^{-2}, a V_{OC} of 0.96 V, and an FF of 0.80, resulting in a PCE of 13.64%. For comparison, a J_{SC} of 14.00 mA cm^{-2}, a V_{OC} of 0.93 V, an FF of 0.80, and a PCE of 10.35% are exhibited by the best performance device with the air-annealed PEDOT:PSS HTL. The series resistance of both devices are similar, which could be attributed to similar quality of the perovskite films and the close electrical conductivity of air-annealed and toluene vapor-annealed PEDOT:PSS HTLs. The almost doubled shunt resistance of the device with the toluene vapor-annealed PEDOT:PSS HTL indicates more balanced charge transport and collection rates because of the better energy alignment (Figure 5c), yielding a higher V_{OC} and J_{SC}. The best performance device with the EG-washed PEDOT:PSS HTL shows the decrease in J_{SC} and FF to 11.27 mA cm^{-2} and 0.70, respectively, leading to a PCE of 7.39%. The result indicates that a high electrical conductivity of HTLs does not ensure a high device performance of perovskite solar cells, which has been reported in the previous work.[35] Even though the series resistance of the device with the EG-washed PEDOT:PSS is 4.83 Ω cm^2, which is the lowest among three types of devices because of its extremely high electrical conductivity (Figure 5a), the significantly decreased shunt resistance, 128.95 Ω cm^2, results in a low J_{SC} and FF of the device, which could be partially attributed to the larger energy misalignment (Figure 5c). There are no observable hysteresis in the forward and backward scans of the $J-V$ curves for the devices with the air-annealed and toluene vapor-annealed PEDOT:PSS HTLs. However, a significant hysteresis is observed when a reverse bias is applied to the device with the EG-washed PEDOT:PSS HTL. Previous study shows that the PSS-rich layer on the surface of PEDOT:PSS films has an electron blocking effect.[49] The absence of the PSS-rich layer makes the EG-washed PEDOT:PSS HTL ineffectively block electron injection in the reverse bias. As a result, the current density decreases with the decrease in applied reverse voltage during the forward scan (dashed red line in Figure 7b). The higher applied reverse voltage around −0.4 V in the backward scan, where the current density starts to increase with the increase in applied reverse voltage, indicates a built-up internal electric field caused by the accumulated charges at the HTL/perovskite interface.

We further investigated how different PEDOT:PSS HTLs affect charge extraction and recombination in the devices. Figure 7c presents the power law dependence of the J_{SC} with light intensity ($J \propto I^{\alpha}$) in a double logarithmic scale. The value of the scaling exponent α implies the balance of charge generation, transport, and extraction. When α is equal to 1, there is no substantial space charge built up and all carriers are

https://dx.doi.org/10.1021/acsaem.0c01194
ACS Appl. Energy Mater. 2020, 3, 9656−9666

collected prior to recombination. When α is less than 1, this could be a result of bimolecular recombination, variations in hole and electron carrier mobilities, or distribution in the density of states. A scaling exponent $\alpha \sim 0.75$ implies the space charge effect, which might be induced by a carrier imbalance or an interfacial barrier.[50,51] Generally, the monomolecular recombination refers to any first-order process including the geminate recombination of a bound electron−hole pair before dissociation and the Shockley−Read−Hall (SRH) recombination in the interfacial layer, while the bimolecular recombination refers to the recombination of free electrons and holes in the photoactive layer.[52] The α value of the device with the toluene vapor-annealed PEDOT:PSS HTL is the largest one, 0.97, indicating that this HTL significantly mitigates the interfacial recombination loss at the HTL/$CH_3NH_3PbI_3$ interface, thus improving J_{SC}, V_{OC}, and FF. Both devices with air-annealed and EG-washed PEDOT:PSS HTLs show the same α value, 0.93, indicating that multiple effects such as bimolecular recombination and imbalanced hole and electron extraction could coexist, resulting in loss of photogenerated charges and thus lowering J_{SC}.

Because all of the photogenerated charge carriers in the perovskite layer will eventually recombine within the cell under open-circuit conditions,[53] the trend of V_{OC} as a function of light intensity provides a direct insight into the role of trap-assisted recombination within the devices having different HTLs. The slope, nk_BT/q, could be an indicator, where k_B is the Boltzmann constant, T is the absolute temperature, and q is the electron charge. Entirely trap-assisted recombination may be identified by a slope of $2k_BT/q$, while a slope in the order of $1k_BT/q$ is indicative of purely bimolecular recombination under open-circuit conditions.[54] As shown in Figure 7d, among the three devices, the device with the EG-washed PEDOT:PSS HTL has the slope $1.97k_BT/q$, while the other two devices with the air-annealed and toluene vapor-annealed HTLs have the slopes $0.89k_BT/q$ and $0.92k_BT/q$, respectively, which have the n values less than 1. These results clearly reveal that trap-assisted recombination dominates in the device with the EG-washed PEDOT:PSS HTL, resulting in loss of photogenerated charges, lowering J_{SC} and FF. The device with the toluene vapor-annealed PEDOT:PSS HTL has the slope close to $1k_BT/q$, indicating that bimolecular recombination is predominant, resulting in the best J_{SC}.

It is worth to note that the crystallinity of perovskite layers on three HTLs is quite identical, implying similar charge generation and transport rates within the active layers. All the results, from TRPL, forward and backward $J-V$ curves, to light intensity-dependent J_{SC} and V_{OC}, point out that the improved device performance based on the toluene vapor-annealed HTL is mainly attributed to the efficient charge extraction and reduction of the monomolecular SRH recombination at the HTL/perovskite interface. In contrast, despite the fact that the EG-washed PEDOT:PSS film has a 5 orders of magnitude increase in electrical conductivity, the rough and more PEDOT surface could create more trap states at the HTL/perovskite interface, leading to a detrimental performance.

CONCLUSIONS

In summary, we have demonstrated that nonpolar solvent toluene vapor annealing and polar solvent EG washing post treatments result in dramatically different electrical properties, surface morphologies, compositions, and PEDOT structures of PEDOT:PSS thin films compared to the conventional air-annealed PEDOT:PSS thin film. The toluene vapor-annealed PEDOT:PSS film exhibits smooth, PSS-dominated surfaces with slightly increased electrical conductivity and better energetically aligned work function with the valence band maximum of the $CH_3NH_3PbI_3$ perovskite. Consequently, the solar cells with the toluene vapor-annealed PEDOT:PSS HTLs yield the highest J_{SC}, V_{OC}, and FF because of the reduced interfacial charge recombination. In contrast, because the excess PSS is washed off by EG during spin casting, the EG-washed PEDOT:PSS film shows a rough surface with more PEDOT domains. Its electrical conductivity increases by 5 orders of magnitude, but the work function is reduced farther apart from the valence band maximum of $CH_3NH_3PbI_3$ perovskite. As a result, the solar cells with the EG-washed PEDOT:PSS HTLs exhibit the lowest J_{SC} and FF because of the increased trap-assisted recombination at the HTL/perovskite interface. This study sheds light on the modification of PEDOT:PSS HTLs with polar and nonpolar solvent post-treatment and the consequence to charge recombination and extraction at the modified HTL/perovskite interfaces, and therefore, it offers a promising means for further improving the performance of inverted planar perovskite solar cells.

EXPERIMENTAL SECTION

Materials. Lead(II) iodide (PbI_2, 99.9%), toluene (anhydrous, 99.8%), chloroform (≥99.99%), γ-butyrolactone (GBL, ≥99%), *N*,*N*-dimethyl sulfoxide (DMSO, anhydrous, ≥99.9%), and bathocuproine (BCP, 96%) were purchased from Sigma-Aldrich. Ethylene glycol (EG, 99.9%) was purchased from Fisher Scientific. PEDOT:PSS (Clevios P VP AI 4083) was obtained from H.C. Starck. Methylammonium iodide (MAI) was purchased from Greatcell Solar (Queanbeyan, Australia). Phenyl-C_{61}-butyric acid methyl ester ($PC_{60}BM$) (>99.5%) was purchased from American Dye Source (Quebec, Canada). All purchased materials were used without further purification.

Solvent Post-treatment of PEDOT:PSS Films. Glass substrates were cut into 15 mm × 15 mm pieces and cleaned sequentially by sonication in soapy deionized (DI) water, DI water, acetone, and isopropanol for 15 min each and then treated with 100 W oxygen plasma for 10 min. AI 4083 PEDOT:PSS (85 μL) dispersion filtered through a 0.45 μm nylon filter was spin-coated onto a cleaned glass substrate at 5000 rpm for 60 s. For air-annealing samples, the substrates were transferred onto a hot plate and annealed at 120 °C for 25 min. For toluene vapor-annealing samples, the substrates were transferred into a glass Petri dish on a hot plate, and a drop of 200 μL of toluene was added inside the Petri dish, and then, the substrates were annealed inside the covered Petri dish at 120 °C for 25 min. For EG-washing samples, a drop of 70 μL of EG was added on an air-annealed PEDOT:PSS film and spin-coated at 5000 rpm for 60 s and then annealed at 120 °C for another 10 min.

Characterization of PEDOT:PSS Films. The morphology of PEDOT:PSS thin films was characterized by tapping mode atomic force microscopy (TM-AFM) using a digital multimode AFM equipped with a Nanoscope IVa controller. Electrical conductivity was measured using a Jandel cylindrical four-point probe connected with a Keithley 2450 SourceMeter. Film thickness was characterized using an Olympus OLS41 profilometer. Raman spectroscopy measurements were carried out on a Thermo Scientific DXR2 Raman microscope to investigate the chemical structure of PEDOT:PSS. A 532 nm green laser with the laser power between 1 and 5 mW was illuminated and focused through a 50× objective lens onto the polymer thin films. Raman spectra were fitted using Peakfit software with an assumption of 50% Gaussian and 50% Lorentzian component peaks. Contact angles were measured using the First Ten Angstroms (FTA)-100 contact angle and surface tension instrument to investigate surface hydrophobicity.

https://dx.doi.org/10.1021/acsaem.0c01194
ACS Appl. Energy Mater. 2020, 3, 9656−9666

X-ray photoelectron spectroscopy (XPS) measurements were conducted using a Kratos AXIS Ultra DLD X-ray photoelectron spectrometer to investigate the surface composition and chemical states of AI 4083 PEDOT:PSS thin films prepared with air annealing, toluene vapor annealing, and EG washing. The incident X-rays were monochromatized Al Kα (KE = 1486.6 eV) operated at 10 mA and 15 kV. All XPS data were acquired at both a normal photoelectron takeoff angle of 0° and high electron takeoff angle of 70°. The survey spectra were acquired with a step size of 1.0 eV and a dwell time of 100 ms at a spectrometer pass energy of 160 eV. The high-resolution spectra were acquired with a step size of 0.1 eV and a dwell time of 425 ms for S 2p spectra and 259 ms for C 1s spectra at a spectrometer pass energy of 40 eV. Data analysis was performed using Kratos Vision Processing software (ver. 2.2.8). The binding energy scale was calibrated by assigning the lowest binding energy C 1s peak to 285.0 eV. All samples were measured under an ultrahigh vacuum of around 5×10^{-9} Torr.

Ultraviolet photoelectron spectroscopy (UPS) measurements were conducted using a Kratos AXIS Ultra DLD spectrometer to investigate the work function of PEDOT:PSS thin films. A He discharge lamp source (Kratos) at an excitation energy of 21.2 eV was used in combination with a delay line detector at an electron pass energy of 5 eV. The UPS spectra for Au were acquired with a step size of 0.1 eV and a dwell time of 100 ms. The high-resolution UPS spectra and Fermi edge spectra were acquired with a step size of 0.01 eV and a dwell time of 100 ms.

Fabrication of $CH_3NH_3PbI_3$ Perovskite Thin Films. Indium tin oxide (ITO)-coated glass (10 Ω sq^{-1}, Colorado Concept Coatings, LLC) was cut into 15 mm × 15 mm pieces, which were then cleaned following the steps described above for the cleaning of glass substrates. The PEDOT:PSS thin films were prepared with air annealing, toluene vapor annealing, and EG washing as described above, and the substrates were transferred into a N_2 glovebox for making $CH_3NH_3PbI_3$ perovskite films. The $CH_3NH_3PbI_3$ perovskite precursor solutions were prepared by dissolving CH_3NH_3I and PbI_2 at a 1:1 molar ratio in GBL and DMSO (7:3, v/v) with a total concentration of 2.0 M. The precursor was mixed at 70 °C for 2 h and was filtered through a 0.45 μm PTFE filter before use. A 70 μL drop of precursor solution was spin-coated on a cleaned substrate at 1000 rpm for 15 s and 4000 rpm for 45 s in a nitrogen glovebox. A drop of 500 μL of toluene as an antisolvent was in situ dripped onto the substrate during the last 15 s of the second spin-coating step. The $CH_3NH_3PbI_3$ perovskite films were then thermally annealed at 100 °C for 10 min.

Characterization of $CH_3NH_3PbI_3$ Perovskite Thin Films. Scanning electron microscopy (SEM) images were acquired using an FEI Sirion scanning electron microscope operated at 5 kV to determine the surface morphology of $CH_3NH_3PbI_3$ perovskite thin films. Two-dimensional XRD patterns were collected with Bruker GADDS D8 Focus Powder Discover diffractometer using Cu Kα radiation (λ = 1.5419 Å), and the data were processed using the EVA package provided by Burker Axs to investigate the crystalline structures of $CH_3NH_3PbI_3$ perovskite thin films. UV−vis absorption spectra were collected using a Varian Cary 5000 UV−vis−NIR spectrophotometer. The TRPL measurements were taken using a Fluo Time 100 spectrometer by means of time-correlated single photon counting (TSCPC). A 470 nm laser with a pulse width of 70−90 ps was excited from the glass side, and the TRPL decays were measured at a peak emission wavelength of 780 nm.

Fabrication and Characterization of p−i−n Perovskite Solar Cells. The ITO/PEDOT:PSS/$CH_3NH_3PbI_3$ films were fabricated as described above. A $PC_{60}BM$ solution (15 mg mL^{-1} in chloroform) was then spin-coated on the perovskite films at 4000 rpm for 60 s and dried without annealing. Then, a BCP solution (2 mg mL^{-1} in 2-propanol) was spin-coated on the $PC_{60}BM$ films at 4000 rpm for 60 s and dried without annealing. Finally, 16 silver electrodes with a thickness of 150 nm and an area of 3.14×10^{-6} m^2 were thermally evaporated on each substrate through a shadow mask at the background pressure <10^{-6} Torr. The resulting device structure is ITO/PEDOT:PSS/$CH_3NH_3PbI_3$/$PC_{60}BM$/BCP/Ag. The current density−voltage (J−V) characteristic curves were measured in a N_2 glovebox with a Keithley 2400 SourceMeter and a solar simulator with a Solar Light Co. xenon lamp (16S-300W) and an AM 1.5G filter. The light intensity was calibrated to 100 mW cm^{-2} using a calibrated silicon solar cell that had been previously standardized at the National Renewable Energy Laboratory.

■ ASSOCIATED CONTENT

Supporting Information

The Supporting Information is available free of charge at https://pubs.acs.org/doi/10.1021/acsaem.0c01194.

XPS spectra of C 1s of PEDOT:PSS thin films prepared with air annealing, toluene vapor annealing, and EG washing; UV adsorption and transmittance spectra of PEDOT:PSS films prepared with air annealing, toluene vapor annealing, and EG washing; secondary cutoff, Fermi level, and calculated work function from the UPS spectra of PEDOT:PSS thin films prepared with air annealing, toluene vapor annealing, and EG washing; and SEM images and UV−vis absorption spectrum of $CH_3NH_3PbI_3$ perovskite thin films fabricated on air-annealed, toluene vapor-annealed, and EG-washed PEDOT:PSS thin films (PDF)

■ AUTHOR INFORMATION

Corresponding Author

Qiuming Yu − *Department of Chemical Engineering, University of Washington, Seattle, Washington 98195, United States;* orcid.org/0000-0002-2401-4664; Phone: 206-543-4807; Email: qyu@uw.edu; Fax: 206-685-3451

Authors

Zhiyin Niu − *Department of Chemical Engineering, University of Washington, Seattle, Washington 98195, United States;* orcid.org/0000-0002-7686-0707

Erjin Zheng − *Department of Chemical Engineering, University of Washington, Seattle, Washington 98195, United States;* orcid.org/0000-0002-0576-5614

Hao Dong − *Department of Chemical Engineering, University of Washington, Seattle, Washington 98195, United States;* orcid.org/0000-0002-7383-9523

Gabriella A. Tosado − *Department of Chemical Engineering, University of Washington, Seattle, Washington 98195, United States*

Complete contact information is available at: https://pubs.acs.org/10.1021/acsaem.0c01194

Notes

The authors declare no competing financial interest.

■ ACKNOWLEDGMENTS

The authors gratefully acknowledge financial support provided by the National Science Foundation (CBET 1748101 and CMMI 1661660) and the Defense Threat Reduction Agency (HDTRA1-15-1-0021). Part of this work was conducted at the Washington Nanofabrication Facility/Molecular Analysis Facility, a National Nanotechnology Coordinated Infrastructure (NNCI) site at the University of Washington (UW), which is supported in part by funds from the National Science Foundation (awards NNCI-1542101, 1337840, and 0335765), the National Institutes of Health, the Molecular Engineering & Sciences Institute, the Clean Energy Institute, the Washington Research Foundation, the M. J. Murdock

Charitable Trust, Altatech, ClassOne Technology, GCE Market, Google, and SPTS. Some device fabrication steps and the measurements of UV−vis absorption and photoluminescence were carried out in the UW Department of Chemistry's Photonics Research Center and the facility of Spectroscopic. Raman spectra were taken using the Raman instrument in the Biochemical Diagnostics Foundry for Translational Research supported by the M.J. Murdock Charitable Trust.

REFERENCES

(1) Hoke, E. T.; Slotcavage, D. J.; Dohner, E. R.; Bowring, A. R.; Karunadasa, H. I.; McGehee, M. D. Reversible Photo-Induced Trap Formation in Mixed-Halide Hybrid Perovskites for Photovoltaics. *Chem. Sci.* **2015**, *6*, 613−617.

(2) Wehrenfennig, C.; Eperon, G. E.; Johnston, M. B.; Snaith, H. J.; Herz, L. M. High Charge Carrier Mobilities and Lifetimes in Organolead Trihalide Perovskites. *Adv. Mater.* **2014**, *26*, 1584−1589.

(3) Shi, D.; Adinolfi, V.; Comin, R.; Yuan, M.; Alarousu, E.; Buin, A.; Chen, Y.; Hoogland, S.; Rothenberger, A.; Katsiev, K.; Losovyj, Y.; Zhang, X.; Dowben, P. A.; Mohammed, O. F.; Sargent, E. H.; Bakr, O. M. Low Trap-State Density and Long Carrier Diffusion in Organolead Trihalide Perovskite Single Crystals. *Science* **2015**, *347*, 519−522.

(4) Xing, G.; Mathews, N.; Sun, S.; Lim, S. S.; Lam, Y. M.; Gratzel, M.; Mhaisalkar, S.; Sum, T. C. Long-Range Balanced Electron- and Hole-Transport Lengths in Organic-Inorganic CH3NH3PbI3. *Science* **2013**, *342*, 344−347.

(5) Stranks, S. D.; Eperon, G. E.; Grancini, G.; Menelaou, C.; Alcocer, M. J. P.; Leijtens, T.; Herz, L. M.; Petrozza, A.; Snaith, H. J. Electron-Hole Diffusion Lengths Exceeding 1 Micrometer in an Organometal Trihalide Perovskite Absorber. *Science* **2013**, *342*, 341−344.

(6) Jiang, Q.; Zhao, Y.; Zhang, X.; Yang, X.; Chen, Y.; Chu, Z.; Ye, Q.; Li, X.; Yin, Z.; You, J. Surface Passivation of Perovskite Film for Efficient Solar Cells. *Nat. Photonics* **2019**, *13*, 460−466.

(7) Kojima, A.; Teshima, K.; Shirai, Y.; Miyasaka, T. Organometal Halide Perovskites as Visible-Light Sensitizers for Photovoltaic Cells. *J. Am. Chem. Soc.* **2009**, *131*, 6050−6051.

(8) Bai, Y.; Meng, X.; Yang, S. Interface Engineering for Highly Efficient and Stable Planar p-i-n Perovskite Solar Cells. *Adv. Energy Mater.* **2018**, *8*, 1701883−1701896.

(9) Meng, L.; You, J.; Guo, T.-F.; Yang, Y. Recent Advances in the Inverted Planar Structure of Perovskite Solar Cells. *Acc. Chem. Res.* **2016**, *49*, 155−165.

(10) de Kok, M. M.; Buechel, M.; Vulto, S. I. E.; van de Weijer, P.; Meulenkamp, E. A.; de Winter, S. H. P. M.; Mank, A. J. G.; Vorstenbosch, H. J. M.; Weijtens, C. H. L.; van Elsbergen, V. Modification of PEDOT:PSS as hole injection layer in polymer LEDs. *Phys. Status Solidi A* **2004**, *201*, 1342−1359.

(11) Zheng, E.; Zhang, X.; Esopi, M. R.; Cai, C.; Zhou, B.; Lin, Y.-Y.; Yu, Q. Narrowband Ultraviolet Photodetectors Based on Nanocomposite Thin Films with High Gain and Low Driving Voltage. *ACS Appl. Mater. Interfaces* **2018**, *10*, 41552−41561.

(12) Zhang, X.; Zheng, E.; Esopi, M. R.; Cai, C.; Yu, Q. Flexible Narrowband Ultraviolet Photodetectors with Photomultiplication Based on Wide Band Gap Conjugated Polymer and Inorganic Nanoparticles. *ACS Appl. Mater. Interfaces* **2018**, *10*, 24064−24074.

(13) Crispin, X.; Marciniak, S.; Osikowicz, W.; Zotti, G.; Van der Gon, A. W. D.; Louwet, F.; Fahlman, M.; Groenendaal, L.; De Schryver, F.; Salaneck, W. R. Conductivity, Morphology, Interfacial Chemistry, and Stability of Poly(3,4-Ethylene Dioxythiophene)-Poly(Styrene Sulfonate): A Photoelectron Spectroscopy Study. *J. Polym. Sci., Part B: Polym. Phys.* **2003**, *41*, 2561−2583.

(14) Higgins, A. M.; Martin, S. J.; Jukes, P. C.; Geoghegan, M.; Jones, R. A. L.; Langridge, S.; Cubitt, R.; Kirchmeyer, S.; Wehrum, A.; Grizzi, I. Interfacial Structure in Semiconducting Polymer Devices. *J. Mater. Chem.* **2003**, *13*, 2814−2818.

(15) Hwang, J.; Amy, F.; Kahn, A. Spectroscopic study on sputtered PEDOT·PSS: Role of surface PSS layer. *Org. Electron.* **2006**, *7*, 387−396.

(16) Greczynski, G.; Kugler, T.; Keil, M.; Osikowicz, W.; Fahlman, M.; Salaneck, W. R. Photoelectron Spectroscopy of Thin Films of PEDOT-PSS Conjugated Polymer Blend: a Mini-Review and Some New Results. *J. Electron Spectrosc. Relat. Phenom.* **2001**, *121*, 1−17.

(17) Elschner, A. *PEDOT: Principles and Applications of an Intrinsically Conductive Polymer*; CRC Press: Boca Raton, FL, 2011.

(18) Jönsson, S. K. M.; Birgerson, J.; Crispin, X.; Greczynski, G.; Osikowicz, W.; Denier van der Gon, A. W.; Salaneck, W. R.; Fahlman, M. The effects of solvents on the morphology and sheet resistance in poly(3,4-ethylenedioxythiophene)-polystyrenesulfonic acid (PEDOT-PSS) films. *Synth. Met.* **2003**, *139*, 1−10.

(19) Nevrela, J.; Micjan, M.; Novota, M.; Kovacova, S.; Pavuk, M.; Juhasz, P.; Kovac, J.; Jakabovic, J.; Weis, M. Secondary Doping in Poly(3,4-Ethylenedioxythiophene):Poly(4-Styrenesulfonate) Thin Films. *J. Polym. Sci., Part B: Polym. Phys.* **2015**, *53*, 1139−1146.

(20) Ouyang, J. "Secondary Doping" Methods to Significantly Enhance the Conductivity of PEDOT:PSS for Its Application As Transparent Electrode of Optoelectronic Devices. *Displays* **2013**, *34*, 423−436.

(21) Yeo, J.-S.; Yun, J.-M.; Kim, D.-Y.; Park, S.; Kim, S.-S.; Yoon, M.-H.; Kim, T.-W.; Na, S.-I. Significant Vertical Phase Separation in Solvent-Vapor-Annealed Poly(3,4-ethylenedioxythiophene):Poly-(styrene sulfonate) Composite Films Leading to Better Conductivity and Work Function for High-Performance Indium Tin Oxide-Free Optoelectronics. *ACS Appl. Mater. Interfaces* **2012**, *4*, 2551−2560.

(22) Kim, J. Y.; Jung, J. H.; Lee, D. E.; Joo, J. Enhancement of electrical conductivity of poly(3,4-ethylenedioxythiophene)/poly(4-styrenesulfonate) by a change of solvents. *Synth. Met.* **2002**, *126*, 311−316.

(23) Sun, K.; Li, P.; Xia, Y.; Chang, J.; Ouyang, J. Transparent Conductive Oxide-Free Perovskite Solar Cells with PEDOT:PSS as Transparent Electrode. *ACS Appl. Mater. Interfaces* **2015**, *7*, 15314−15320.

(24) Huang, X.; Wang, K.; Yi, C.; Meng, T.; Gong, X. Efficient Perovskite Hybrid Solar Cells by Highly Electrical Conductive PEDOT:PSS Hole Transport Layer. *Adv. Energy Mater.* **2016**, *6*, 1501773−1501780.

(25) Zhang, S.; Yu, Z.; Li, P.; Li, B.; Isikgor, F. H.; Du, D.; Sun, K.; Xia, Y.; Ouyang, J. Poly(3,4-Ethylenedioxythiophene):Polystyrene Sulfonate Films With Low Conductivity And Low Acidity Through a Treatment of Their Solutions With Probe Ultrasonication And Their Application As Hole Transport Layer in Polymer Solar Cells And Perovskite Solar Cells. *Org. Electron.* **2016**, *32*, 149−156.

(26) Thomas, J. P.; Zhao, L.; McGillivray, D.; Leung, K. T. High-efficiency hybrid solar cells by nanostructural modification in PEDOT:PSS with co-solvent addition. *J. Mater. Chem. A* **2014**, *2*, 2383−2389.

(27) Wang, Q.; Chueh, C.-C.; Eslamian, M.; Jen, A. K.-Y. Modulation of PEDOT:PSS pH for Efficient Inverted Perovskite Solar Cells with Reduced Potential Loss and Enhanced Stability. *ACS Appl. Mater. Interfaces* **2016**, *8*, 32068−32076.

(28) Huang, D.; Goh, T.; Kong, J.; Zheng, Y.; Zhao, S.; Xu, Z.; Taylor, A. D. Perovskite solar cells with a DMSO-treated PEDOT:PSS hole transport layer exhibit higher photovoltaic performance and enhanced durability. *Nanoscale* **2017**, *9*, 4236−4243.

(29) Sun, K.; Xia, Y.; Ouyang, J. Improvement in The Photovoltaic Efficiency of Polymer Solar Cells by Treating the Poly(3,4-Ethylenedioxythiophene):Poly(Styrenesulfonate) Buffer Layer With Co-Solvents of Hydrophilic Organic Solvents and Hydrophobic 1,2-Dichlorobenzene. *Sol. Energy Mater. Sol. Cells* **2012**, *97*, 89−96.

(30) Syed, A. a.; Poon, C. Y.; Li, H. W.; Zhu, F. A Sodium Citrate-Modified-PEDOT:PSS Hole Transporting Layer for Performance Enhancement in Inverted Planar Perovskite Solar Cells. *J. Mater. Chem. C* **2019**, *7*, 5260−5266.

(31) Shahbazi, S.; Tajabadi, F.; Shiu, H.-S.; Sedighi, R.; Jokar, E.; Gholipour, S.; Taghavinia, N.; Afshar, S.; Diau, E. W.-G. An Easy

https://dx.doi.org/10.1021/acsaem.0c01194
ACS Appl. Energy Mater. 2020, 3, 9656−9666

Method to Modify PEDOT:PSS/Perovskite Interfaces for Solar Cells With Efficiency Exceeding 15%. *RSC Adv.* **2016**, *6*, 65594−65599.
(32) Xia, Y.; Sun, K.; Chang, J.; Ouyang, J. Effects of organic inorganic hybrid perovskite materials on the electronic properties and morphology of poly(3,4-ethylenedioxythiophene):poly-(styrenesulfonate) and the photovoltaic performance of planar perovskite solar cells. *J. Mater. Chem. A* **2015**, *3*, 15897−15904.
(33) Niu, Q.; Huang, W.; Tong, J.; Lv, H.; Deng, Y.; Ma, Y.; Zhao, z.; Xia, R.; Zeng, W.; Min, Y.; huang, W. Understanding the mechanism of PEDOT: PSS modification via solvent on the morphology of perovskite films for efficient solar cells. *Synth. Met.* **2018**, *243*, 17−24.
(34) Liu, H.; Li, X.; Zhang, L.; Hong, Q.; Tang, J.; Zhang, A.; Ma, C.-Q. Influence of The Surface Treatment of PEDOT:PSS Layer With High Boiling Point Solvent On The Performance of Inverted Planar Perovskite Solar Cells. *Org. Electron.* **2017**, *47*, 220−227.
(35) Li, X.-Y.; Zhang, L.-P.; Tang, F.; Bao, Z.-M.; Lin, J.; Li, Y.-Q.; Chen, L.; Ma, C.-Q. The solvent treatment effect of the PEDOT:PSS anode interlayer in inverted planar perovskite solar cells. *RSC Adv.* **2016**, *6*, 24501−24507.
(36) Reza, K. M.; Gurung, A.; Bahrami, B.; Mabrouk, S.; Elbohy, H.; Pathak, R.; Chen, K.; Chowdhury, A. H.; Rahman, M. T.; Letourneau, S.; Yang, H.-C.; Saianand, G.; Elam, J. W.; Darling, S. B.; Qiao, Q. Tailored PEDOT:PSS Hole Transport Layer for Higher Performance in Perovskite Solar Cells: Enhancement of Electrical and Optical Properties With Improved Morphology. *J. Energy Chem.* **2020**, *44*, 41−50.
(37) Hu, L.; Li, M.; Yang, K.; Xiong, Z.; Yang, B.; Wang, M.; Tang, X.; Zang, Z.; Liu, X.; Li, B.; Xiao, Z.; Lu, S.; Gong, H.; Ouyang, J.; Sun, K. PEDOT:PSS Monolayers to Enhance The Hole Extraction And Stability of Perovskite Solar Cells. *J. Mater. Chem. A* **2018**, *6*, 16583−16589.
(38) Crispin, X.; Jakobsson, F. L. E.; Crispin, A.; Grim, P. C. M.; Andersson, P.; Volodin, A.; van Haesendonck, C.; Van der Auweraer, M.; Salaneck, W. R.; Berggren, M. The Origin of the High Conductivity of Poly(3,4-ethylenedioxythiophene)−Poly-(styrenesulfonate) (PEDOT−PSS) Plastic Electrodes. *Chem. Mater.* **2006**, *18*, 4354−4360.
(39) Ghosh, S.; Inganäs, O. Nano-Structured Conducting Polymer Network Based on PEDOT-PSS. *Synth. Met.* **2001**, *121*, 1321−1322.
(40) Nardes, A. M.; Kemerink, M.; Janssen, R. A. J. Anisotropic Hopping Conduction in Spin-Coated PEDOT : PSS Thin Films. *Phys. Rev. B: Condens. Matter Mater. Phys.* **2007**, *76*, 085208−085214.
(41) Ouyang, J.; Xu, Q.; Chu, C.-W.; Yang, Y.; Li, G.; Shinar, J. On the mechanism of conductivity enhancement in poly(3,4-ethylenedioxythiophene):poly(styrene sulfonate) film through solvent treatment. *Polymer* **2004**, *45*, 8443−8450.
(42) Farah, A. A.; Rutledge, S. A.; Schaarschmidt, A.; Lai, R.; Freedman, J. P.; Helmy, A. S. Conductivity Enhancement of Poly(3,4-Ethylenedioxythiophene)-Poly(Styrenesulfonate) Films Post-Spin-casting. *J. Appl. Phys.* **2012**, *112*, 113709−113716.
(43) Garreau, S.; Louarn, G.; Buisson, J. P.; Froyer, G.; Lefrant, S. In Situ Spectroelectrochemical Raman Studies of Poly(3,4-Ethylenedioxythiophene) (PEDT). *Macromolecules* **1999**, *32*, 6807−6812.
(44) Chiu, W. W.; Travaš-Sejdić, J.; Cooney, R. P.; Bowmaker, G. A. Studies of dopant effects in poly(3,4-ethylenedi-oxythiophene) using Raman spectroscopy. *J. Raman Spectrosc.* **2006**, *37*, 1354−1361.
(45) Łapkowski, M.; Proń, A. Electrochemical oxidation of poly(3,4-ethylenedioxythiophene) — "in situ" conductivity and spectroscopic investigations. *Synth. Met.* **2000**, *110*, 79−83.
(46) Park, H.; Lee, S. H.; Kim, F. S.; Choi, H. H.; Cheong, I. W.; Kim, J. H. Enhanced thermoelectric properties of PEDOT:PSS nanofilms by a chemical dedoping process. *J. Mater. Chem. A* **2014**, *2*, 6532−6539.
(47) Baikie, T.; Fang, Y.; Kadro, J. M.; Schreyer, M.; Wei, F.; Mhaisalkar, S. G.; Graetzel, M.; White, T. J. Synthesis and crystal chemistry of the hybrid perovskite (CH3NH3)PbI3 for solid-state sensitised solar cell applications. *J. Mater. Chem. A* **2013**, *1*, 5628−5641.
(48) Son, D.-Y.; Lee, J.-W.; Choi, Y.-J.; Jang, I.-H.; Lee, S.; Yoo, P. J.; Shin, H.; Ahn, N.; Choi, M.; Kim, D.; Park, N.-G. Self-Formed Grain Boundary Healing Layer for Highly Efficient $CH_3NH_3PbI_3$Perovskite Solar Cells. *Nat. Energy* **2016**, *1*, 1−8.
(49) Mauger, S. A.; Chang, L.; Rochester, C. W.; Moulé, A. J. Directional Dependence of Electron Blocking in PEDOT:PSS. *Org. Electron.* **2012**, *13*, 2747−2756.
(50) Riedel, I.; Parisi, J.; Dyakonov, V.; Lutsen, L.; Vanderzande, D.; Hummelen, J. C. Effect of Temperature And Illumination on The Electrical Characteristics of Polymer-Fullerene Bulk-Heterojunction Solar Cells. *Adv. Funct. Mater.* **2004**, *14*, 38−44.
(51) Zhang, H.; Cheng, J.; Lin, F.; He, H.; Mao, J.; Wong, K. S.; Jen, A. K.-Y.; Choy, W. C. H. Pinhole-Free and Surface-Nanostructured NiOx Film by Room-Temperature Solution Process for High-Performance Flexible Perovskite Solar Cells with Good Stability and Reproducibility. *ACS Nano* **2016**, *10*, 1503−1511.
(52) Jung, J. W.; Chueh, C.-C.; Jen, A. K.-Y. High-Performance Semitransparent Perovskite Solar Cells with 10% Power Conversion Efficiency and 25% Average Visible Transmittance Based on Transparent CuSCN as the Hole-Transporting Material. *Adv. Energy Mater.* **2015**, *5*, 1500486−1500492.
(53) You, J.; Yang, Y.; Hong, Z.; Song, T.-B.; Meng, L.; Liu, Y.; Jiang, C.; Zhou, H.; Chang, W.-H.; Li, G.; Yang, Y. Moisture Assisted Perovskite Film Growth For High Performance Solar Cells. *Appl. Phys. Lett.* **2014**, *105*, 18902−18906.
(54) Shao, S.; Chen, Z.; Fang, H.-H.; ten Brink, G. H.; Bartesaghi, D.; Adjokatse, S.; Koster, L. J. A.; Kooi, B. J.; Facchetti, A.; Loi, M. A. N-type Polymers as Electron Extraction Layers in Hybrid Perovskite Solar Cells With Improved Ambient Stability. *J. Mater. Chem. A* **2016**, *4*, 2419−2426.

https://dx.doi.org/10.1021/acsaem.0c01194
ACS Appl. Energy Mater. 2020, 3, 9656−9666